Photodissociation of Vibrationally Excited Pernitric Acid: HO_2NO_2 ($2\nu_1$) + 390 nm†

Jamie Matthews, Ramesh Sharma, and Amitabha Sinha*

Department of Chemistry and Biochemistry, University of California−San Diego, 9500 Gilman Drive, La Jolla, California 92093-0314

Received: April 8, 2004

Pernitric acid (HO_2NO_2) molecule vibrationally excited in the vicinity of its first OH stretching overtone ($2\nu_1$) is dissociated via electronic excitation using 390-nm light. The nascent energy distribution of the resulting OH fragments is probed by using laser-induced fluorescence at sub-Doppler resolution. We find that for the minor OH + NO_3 channel, 55% of the ~19 600 $cm^{-1}$of available energy goes into relative translation of the two fragments and 45% into internal excitation. In addition, electronically excited NO_2 associated with the dominant HO_2 + NO_2 channel is also observed. The visible fluorescence from the excited NO_2 fragments is sufficiently intense to allow vibrational action spectra of HO_2NO_2 to be recorded with good signal-to-noise. As vibrational states in the vicinity of the $2\nu_1$ level can also undergo unimolecular dissociation on the ground electronic surface, comparing relative integrated intensities of spectral features appearing in the vibrational state selected action spectra with their known total infrared absorption cross sections provides a means for estimating unimolecular dissociation quantum yields from these levels under collision-free conditions. The present results indicate that at 298 K the unimolecular dissociation quantum yield for the HO_2NO_2 ($2\nu_1$) state is ~30 ± 5%. Evidence is also presented for the generation of HOONO impurity in the standard synthesis route for HO_2NO_2.

Introduction

Peroxynitric acid (PNA/HO_2NO_2) is formed in the atmosphere via a three-body recombination reaction involving the HO_2 and NO_2 radicals and, hence, provides a temporary reservoir for these species.[1] Apart from its reaction with OH, photodissociation constitutes an important removal mechanism for atmospheric HO_2NO_2. The relatively weak HO_2-NO_2 bond strength implies that PNA molecules can be dissociated not only via the absorption of UV photons, associated with promotion to a repulsive excited electronic state, but also through unimolecular dissociation initiated by infrared excitation on its ground electronic surface.[2,3] The latter mechanism is expected to be important, for example, at high solar zenith angles (>90°) where the extended optical path lengths lead to selective depletion of the short wavelength component in the solar actinic flux relative to the longer wavelengths due to scattering and absorption.[4−6] Thus, to fully quantify the photochemical loss mechanisms of atmospheric PNA, a thorough understanding of both its vibrational and electronic photochemistry is needed.

The UV absorption spectrum of PNA has been investigated by several groups and consists of a broad absorption feature starting around 360 nm and extending well below 190 nm.[7−9] Ab initio calculations[10] suggest the presence of two excited singlet electronic states in the near-UV region both of which are dissociative along the HO_2-NO_2 and the $HO-ONO_2$ coordinates. The first excited singlet state, 2^1A, is located 5.05 eV above the ground state while the second is at 5.52 eV. Quantum yield measurements from the photodissociation of PNA have been investigated at 248 nm and indicate that the primary channels are those associated with the formation of OH and HO_2 photofragments, even though energetically several other dissociation pathways are also possible at this wavelength. Specifically, the measurements of Rohel et al.[10] at 248 nm find the following quantum yields:

$$HO_2NO_2 \rightarrow OH + NO_3\ (34\%) \qquad (1a)$$

$$\rightarrow HO_2 + NO_2\ (56\%) \qquad (1b)$$

The quantum yields for the above two channels were determined by respectively measuring the *total yield* of OH and NO_2 fragments resulting from 248-nm photolysis and thus do not preclude the possibility that some of the fragments shown in the above equations are formed in excited electronic states. In fact emission from electronically excited NO_2 has been reported in the 248-nm photodissociation study of Macleod et al.[11]

Dissociation of PNA can also occur readily on its ground electronic surface and several aspects of this unimolecular reaction have been investigated both experimentally and theoretically.[6,12−14] Using available thermo chemical data,[9] one readily estimates the threshold energies for opening the lowest energy product channel from simple bond fission of PNA, HO_2 + NO_2 to be ~8110 cm^{-1}. The threshold for opening the HO + NO_3 channel is much higher at ~13 780 cm^{-1}. The difference between the threshold energy for opening the HO_2 + NO_2 channel, 8110 cm^{-1}, and the band center for exciting the first OH stretching overtone ($2\nu_1$) of PNA, 6910 cm^{-1},[15] suggests that unimolecular dissociation can occur upon excitation to the $2\nu_1$ level only with the assistance of substantial thermal energy. At room temperature (298 K) the average internal thermal energy (vib. + rot.) in PNA is estimated to be 700 cm^{-1}.[16] Thus, only states associated with the high-energy tail of the Boltzmann distribution have sufficient energy to make up the ~1200 cm^{-1} energy deficit required to open the HO_2 + NO_2 pathway. Roehl et al. have investigated the quantum yield for unimolecular dissociation of PNA upon excitation to several vibrational levels in the vicinity of the $2\nu_1$ band as a function of temperature and

† Part of the special issue "Richard Bersohn Memorial Issue".

10.1021/jp040285s CCC: $27.50 © 2004 American Chemical Society
Published on Web 08/04/2004

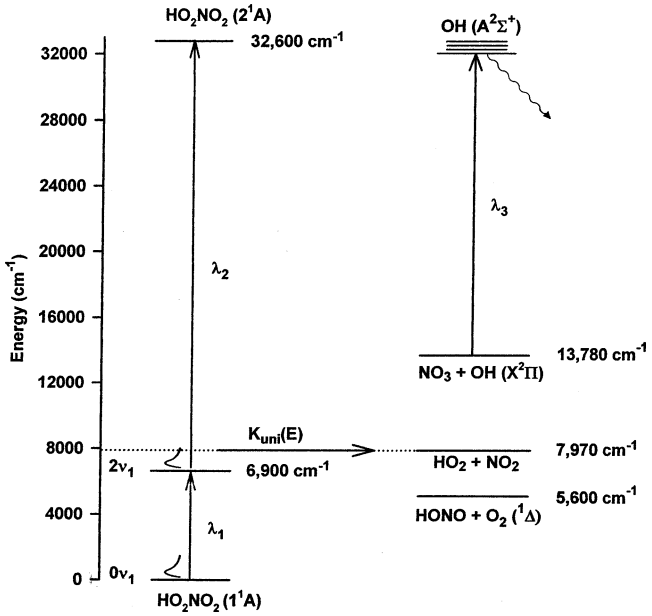

Figure 1. Schematic energy level diagram illustrating photodissociation of vibrationally excited HO_2NO_2 (PNA). Laser λ_1 vibrationally excites room-temperature PNA molecules to the $2\nu_1$ level where λ_2 subsequently further promotes these state-selected molecules to a dissociative electronic excited state. The resulting OH photofragments are probed via LIF by using λ_3. PNA molecules excited to states of the $2\nu_1$ vibrational level having sufficient initial thermal energy can also undergo unimolecular dissociation on the ground electronic surface. The threshold energies for opening the various product channels shown are estimated by using the enthalpy data of refs 6 and 9.

pressure.[6] Consistent with the energy constraints noted above they find that at 295 K, corresponding to the upper limit of their reported temperature range, the quantum yield for unimolecular dissociation for the $2\nu_1$ band is ~27% and independent of pressure over the 2−40 Torr range used in their study.[6]

An invariable complication associated with investigating the laboratory photochemistry of PNA is the presence of impurities. Previous studies have identified H_2O_2, HNO_3, and NO_2 as being the major impurities present in PNA samples generated by using the traditional synthesis route involving $H_2O_2 + NO_2BF_4$.[6,7,15,17] In this study we present evidence that HOONO can also form during the synthesis of PNA. As many of the above impurities have overlapping absorption bands and give rise to common photofragments, great care is needed to ensure that contribution from impurity photochemistry is kept to negligible levels. Below we present the first results of using vibrational state selection to selectively excite and investigate the near-UV photochemistry of PNA while minimizing interference from these impurities. Figure 1 illustrates the approach used in these double-resonance experiments. Infrared light (λ_1) is used to vibrationally state select PNA molecules by excitation in the vicinity of the $2\nu_1$ band, and the vibrationally excited molecules are then subsequently dissociated by promotion to an electronic excited state by using a second photon at ~390 nm (λ_2). Finally the OH fragments resulting from the photodissociation are probed by laser-induced fluorescence with use of a third laser (λ_3). Thus the effective total energy imparted to the PNA molecule through the double-resonance excitation corresponds to an equivalent single photon excitation energy of ~307 nm. Apart from obtaining information regarding the electronic photochemistry of PNA, the double-resonance technique also provides the means for probing several aspects of the unimolecular dissociation dynamics occurring on the ground electronic surface. In particular, fixing λ_2 and λ_3 while varying the wavelength of the infrared excitation laser (λ_1) generates vibrational action spectra that reveal information about the fraction of states within the selected vibrational level that *do not* undergo unimolecular dissociation and thus survive for at least a time period set by the time delay between λ_1 and λ_2. As we discuss below, comparing vibrational band intensities appearing in these double-resonance action spectra with their known total integrated infrared absorption cross sections provides a means for estimating the unimolecular dissociation quantum yields of the bands in the absence of collisions.

Experimental Section

The experimental apparatus is similar to that used in our previous studies investigating unimolecular dissociation of HOCl.[18] Briefly, the photolysis chamber consists of a glass cell equipped with a viewing window for monitoring laser-induced fluorescence (LIF), two sets of mutually orthogonal sidearms for introducing laser light, and several inlet ports for adding reagents. The inside of the cell is coated with halocarbon wax to minimize sample wall loss. We generate HO_2NO_2 (PNA) in a manner similar to that described in the literature using the following reaction scheme:[7,17]

$$H_2O_2 + BF_4NO_2 \rightarrow HO_2NO_2 + HF + BF_3 \qquad (2)$$

The above synthesis is realized in practice by slowly adding ~2 g of BF_4NO_2 to 5 mL of precooled H_2O_2 (~90%) kept in a jacketed glass cell maintained at −13 °C using a chiller circulating an ethylene glycol−water mixture. The entire reaction is conducted inside a glovebag filled with dry N_2. Immediately after the synthesis the sample cell is capped off, removed from the glovebag, and further cooled to −17 °C. The sample cell is then pumped on to remove volatile species such as N_2 and NO_2. During the experimental runs the chiller reservoir temperature is maintained between −13 and −10 °C to regulate the partial pressure of HO_2NO_2 in the sample cell. The HO_2NO_2 sample is slowly flowed into the photolysis cell and varying the extent to which a two-inch diameter bellows valve, connecting the photolysis cell to a mechanical vacuum pump, is opened regulates the pressure. Although the sample reservoir is kept cold, the photolysis cell is at room temperature and typically operates in the pressure range between ~80 and 100 mTorr. All components coming in contact with the reagent prior to entering the photolysis cell are made of either glass or Teflon to minimize loss of PNA. Under typical operating conditions, the PNA samples last about 7−10 days before requiring replacement. Concentrated H_2O_2 used in the synthesis is prepared by bubbling N_2 through a 50% H_2O_2 solution over a period of several days to remove the more volatile water component; the final H_2O_2 concentration is estimated by noting its volume change.

Infrared radiation (λ_1) for exciting the first OH stretching overtone of PNA ($2\nu_1$) is generated by an optical parametric oscillator (OPO: Spectra Physics MOPO-730), which is pumped by the third harmonic of an injection seeded Nd:YAG laser (Spectra Physics GCR-270). The idler beam from the OPO laser provides the required tunable radiation between 6600 and 7150 cm^{-1} with a bandwidth of ~0.4 cm^{-1} and pulse energies ranging from 4 to 6 mJ. Radiation at ~390 nm for exciting the electronic transition in the second step of the double resonance (λ_2) is generated by frequency mixing the visible output of another Nd:YAG laser pumped dye laser operating with R-640 dye with the Nd:Yag laser's fundamental. Typical output pulse energies

from the mixing process are between 8 and 10 mJ. The OH photofragments resulting from the double-resonance excitation are probed via the A−X transition at ∼308 nm with use of laser induced fluorescence (LIF). The 308-nm radiation, which has a bandwidth of 0.17 cm^{-1}, is generated by frequency doubling the output of a third Nd:YAG laser (Continuum: NY81-20) pumped dye laser (Continuum: ND60). The probe and photolysis laser beams are combined on a dichroic mirror and directed into the photolysis cell after passing through a collimating lens system. The vibrational excitation laser propagates counter to the other two beams and is focused into the center of the cell by using a 400-mm lens. For some of the Doppler profile measurements, the probe laser is introduced orthogonal to the other two beams. All three laser systems operate at 20 Hz and have temporal widths (fwhm) of ∼7 ns. The time delay between λ_1 and λ_2 is typically fixed at 20 ns, although for experiments probing the unimolecular dissociative lifetime of the vibrational states, this delay is varied between 7 and 50 ns. The probe laser pulse λ_3 typically occur ∼80 ns after the OPO (λ_1) and its intensity is greatly attenuated to avoid saturation of the OH transitions as well as prevent photolysis of the PNA. The OH fluorescence excited by the probe laser is collected by using an f/1 lens system and imaged onto an end-on photomultiplier (EMI 9635QB). The combination of a color glass filter (Schott UG-11), a 308-nm interference filter, and a 355-nm edge filter located in front of the photomultiplier provides discrimination against scattered laser light. For detection of NO_2 fluorescence the Schott UG-11 color glass filter is replaced with a GG-420 filter and the 308-nm interference and edge filters are removed. The signal from the PMT is sent to a gated charge integrator (LeCroy, 2249SG ADC) and subsequently digitized and passed to a laboratory computer for storage and analysis.

Results and Discussion

As a first step in using double resonance to investigate the photochemistry of PNA we examine the influence of infrared excitation (λ_1) alone on the sample. The right side of Figure 1 illustrates the simple bond fission pathways associated with the dissociation of HO_2NO_2 (PNA) and their corresponding threshold energies. As noted above, in these room-temperature measurements the initial thermal energy associated with the high energy tail of the Boltzman distribution combined with the $2\nu_1$ photon energy is sufficient for opening the $HO_2 + NO_2$ pathway. By contrast the $OH + NO_3$ channel is not accessible at these vibrational excitation energies. Thus based on energetics we do not expect OH fragments to be generated solely from the infrared excitation of PNA in the $2\nu_1$ spectral region. In actual fact, however, we find that freshly prepared PNA samples do give rise to OH signal when exposed to infrared radiation tuned to the vicinity of the $2\nu_1$ vibration. Monitoring the yield of the OH fragments by using the $Q_1(2)$ transition, for example, while scanning the wavelength of the infrared excitation laser (λ_1), generates an action spectrum like the one shown in Figure 2a. We believe that this signal is due to OH fragment generated through the unimolecular dissociation of HOONO impurity present in the PNA sample. Not only is the thermochemistry for opening the HOONO → OH + NO_2 ($D_0 \approx 19.8$ kcal/mol)[19,20] consistent with the energy associated with the $2\nu_1$ excitation, but also the band centers of the four primary spectral features observed in Figure 2a match up exactly with those recently reported in ref 21 for HOONO generated by using the high-pressure three-body recombination reaction: OH + NO_2 + M → HOONO + M. To facilitate a more direct comparison,

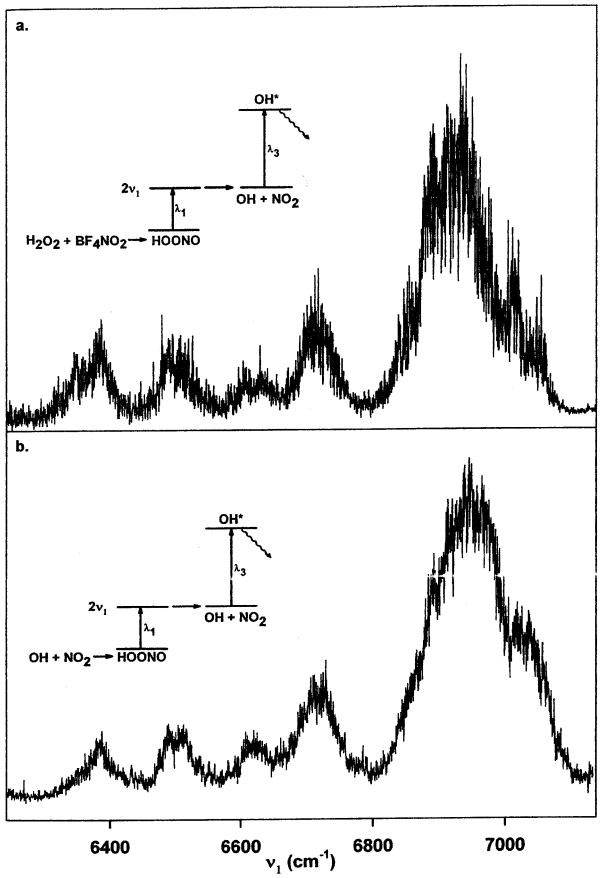

Figure 2. (a) HOONO ($2\nu_1$) action spectrum arising from the H_2O_2 + BF_4NO_2 source. The spectrum is generated by scanning the IR laser (λ_1) while monitoring OH fragment yield through the $Q_1(2)$ transition (λ_3). (b) HOONO($2\nu_1$) action spectrum generated from the HO + NO_2 + M three-body recombination reaction. The OH radicals required for the three-body reaction are generated by using the H + NO_2 reaction with hydrogen atoms being produced by passing H_2 through a microwave discharge in a sidearm reactor.

we have also generated HOONO using the three-body recombination mechanism and the corresponding action spectrum is shown in Figure 2b. Although we have not characterized all aspects of the HOONO formation, we find that the yield of HOONO from the BF_4NO_2 + H_2O_2 source is typically high when BF_4NO_2 is in slight excess of that reported in the Experimental Section. We note that recent studies have reported generating HOONO by using the reaction of $BF_4NO + H_2O_2$.[22] Hence if BF_4NO was present in our system as an impurity it could account for the formation of HOONO. The HOONO signal from our PNA source remains strong only for the first 1 to 2 days of use of a freshly prepared PNA sample, suggesting that it is rather volatile and disappears following extended pumping. Interestingly, to the best of our knowledge prior studies have not reported detecting HOONO impurity in their PNA samples, although it is clear that its presence can potentially interfere with the study of PNA photochemistry. All experiments on PNA that we report below are conducted after the OH signal from HOONO ($2\nu_1$) reached negligible levels.

After eliminating the HOONO interference we are able to more clearly probe the influence of infrared excitation on PNA itself. As expected on the basis of known thermochemistry and also reported by previous investigators, the 0 → $2\nu_1$ excitation of PNA leads to opening the HO_2 + NO_2 pathway. The production of HO_2 is readily verified by conducting the infrared excitation experiments in the presence of added NO. The

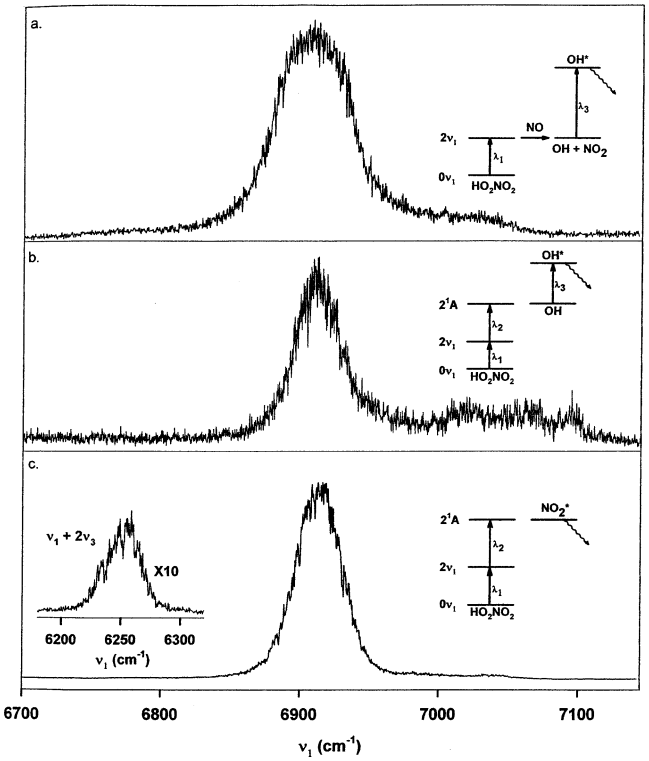

Figure 3. (a) Vibrational overtone action spectrum of HO_2NO_2 ($2\nu_1$). This spectrum is generated by exciting PNA to the $2\nu_1$ level and then converting the unimolecular dissociation products, HO_2, to OH through its reaction with NO, which is also added to the reaction cell. In the spectrum the yield of OH radicals is monitored with the $Q_1(2)$ transition as the $0 \rightarrow 2\nu_1$ excitation frequency is scanned. (b) Vibrational overtone action spectrum of HO_2NO_2 ($2\nu_1$) from the $2\nu_1 + 390$ nm photodissociation. This spectrum is generated by scanning λ_1 while monitoring OH photofragments through the $Q_1(4)$ transition. No nitric oxide is present and the time delay between λ_1 and λ_2 is set at 25 ns. (c) Vibrational overtone action spectrum of HO_2NO_2 ($2\nu_1$) generated via the $2\nu_1 + 390$ nm photodissociation, but monitoring total NO_2 fluorescence while scanning λ_1. The weak $\nu_1 + 2\nu_3$ combination band is shown in the inset. The assignment is from ref 6.

addition of NO initiates the following reaction with the HO_2 photofragments:

$$HO_2 + NO \rightarrow OH + NO_2 \qquad (k = 8.6 \times 10^{-12}\ \text{cm}^3/(\text{molecule s})) \quad (3)$$

Hence this reaction rapidly converts HO_2 to OH and since the latter species can be detected by LIF, the above reaction provides a convenient, although indirect, means for monitoring the formation of HO_2 photofragments. Figure 3a displays a vibrational overtone action spectrum of HO_2NO_2 over the region of the $0 \rightarrow 2\nu_1$ transitions obtained by this method. To facilitate the conversion of HO_2 photofragments to OH, the delay between the probe and vibrational excitation lasers is increased to $\sim$11 μs in these measurements; the resulting OH molecules are monitored via LIF by using the $Q_1(2)$ transition. Comparing Figure 2a and Figure 3a we clearly see that although the HOONO and HO_2NO_2 spectra are distinct, there are substantial regions of overlap in the vicinity of their respective $2\nu_1$ bands. Consequently care must be taken to avoid excitation of the unwanted species.

After examining the predissociation spectra from the $2\nu_1$ vibrational level we focused on the double-resonance excitation experiments. In these measurements, PNA molecules vibrationally excited to the $2\nu_1$ level by the OPO (λ_1) are subsequently further promoted to an electronic excited state by using $\sim$390-nm light (λ_2) (see Figure 1). The choice of wavelength λ_2 is dictated by a desire to maximize the double-resonance signal from PNA while minimizing background signal initiated by λ_2 alone. In particular, the absorption cross-section of both HNO_3 and HOOH is weak at 390 nm and NO_2 is not expected to fluoresce when excited at this wavelength as it leads to dissociation. One advantage of this experimental approach is that the excited electronic state of PNA naturally gives rise to OH fragments, and hence it is not necessary to add nitric oxide to record a vibrational action spectrum. Figure 3b shows a typical vibrational overtone action spectrum of HO_2NO_2 ($2\nu_1$) obtained with the double-resonance technique. The spectrum is generated by scanning λ_1 while monitoring the yield of OH photofragments with use of the $Q_1(4)$ transition. We find that action spectra generated by monitoring yields of other OH rotational states give similar results. In conjunction with the action spectra of PNA, we have also recorded double-resonance spectra of pure HOOH and HNO_3 in separate experiments using the same combination of excitation wavelengths. Through these cross checks we are able to verify that the spectral feature observed at 6910 cm^{-1} in Figure 3b is due to PNA while the feature at 7075 cm^{-1} is due to hydrogen peroxide. Apparently the combination of λ_1 and λ_2 effectively prevents HNO_3 species from contributing at these wavelengths. Thus it is clear that by tuning λ_1 to $\sim$6910 cm^{-1}, the peak of the PNA $2\nu_1$ band, and subsequently photolyzing the vibrationally excited molecules using 390 nm light, we can investigate the near-UV photochemistry of PNA with out interference. We note that the combination of $2\nu_1 + 390$ nm corresponds to an effective single photon excitation of $\sim$307 nm.

Another aspect of the PNA double-resonance action spectra that we have investigated is to examine whether they change as the time delay between λ_1 and λ_2 is varied. By varying this time delay we hoped to probe the lifetime distribution of those states of the $2\nu_{OH}$ vibrational band that have sufficient energy to undergo unimolecular dissociation on the ground electronic surface. Specifically for a given time delay (Δt) between λ_1 and λ_2, only ro-vibrational states that do not undergo unimolecular dissociation during Δt can subsequently interact with λ_2 and produce OH photofragements through promotion to the repulsive electronic excited state. Thus, action spectra of these predissociative vibrational states taken under different time delay settings may exhibit different intensity distributions. The double-resonance action spectrum presented in Figure 3b corresponds to $\Delta t = 25$ ns, and we find that the spectrum does not change noticeably as Δt is reduced to $\sim$7 ns, the temporal resolution limit of our laser system. Thus, these first room-temperature double-resonance measurements suggest that the majority of PNA states that undergo unimolecular dissociation upon excitation through the $0 \rightarrow 2\nu_1$ band apparently do so on a time scale much faster than $\sim$7 ns. This observation is consistent with the lack of pressure dependence reported in the quantum yield measurements of Roehl et al. over the 2−40 Torr range.[6] We also note that the width of the $2\nu_1$ band generated monitoring HO_2 formation by the addition of NO (Figure 3a) is broader than that obtained by using the double-resonance excitation (Figure 3b). We believe this is due to the fact that the action spectrum generated by monitoring unimolecular reaction is biased (due to energy constraint) in favor of states in the $2\nu_1$ band with high internal energy while the action spectra generated by state-selected electronic photodissociation are expected to be equally sensitive to all the states of $2\nu_1$. Using sub-Doppler resolution LIF we have also investigated the energy disposal

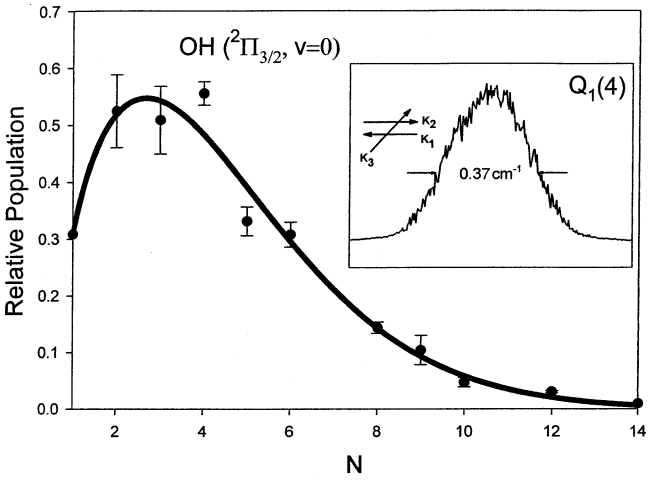

Figure 4. Nascent rotational state distribution of the OH ($v = 0$, $^2\Pi_{3/2}$) manifold resulting from the $2\nu_1 + 390$ nm excitation of PNA. The inset shows the Doppler width associated with the $Q_1(4)$ transition with the 0.17 cm^{-1} probe laser line width convoluted out.

for the OH + NO_3 channel resulting from the double-resonance photodissociation of PNA. Taking into account the photon energies associated with λ_1 and λ_2, the average thermal energy in PNA (700 cm^{-1}), and the bond energy for opening the OH + NO_3 channel (13 780 cm^{-1}), we estimate the available energy associated with this dissociation pathway to be ~19 500 cm^{-1}. By scanning the probe laser over the rotational transitions of the OH fragment's A ← X band and examining both their intensity and Doppler line widths, we find that 470 cm^{-1} of the available energy goes into rotational and 8420 cm^{-1} into translational excitation of the OH fragment. The nascent OH energy disposal results are shown in Figure 4. Within our detection limit, we do not observe any vibrationally excited OH. Applying momentum and energy conservation, we infer that the partner NO_3 fragment receives ~2310 cm^{-1} of translational and ~8250 cm^{-1} of internal excitation. The amount of internal energy available for NO_3 is insufficient to produce it in its electronic excited state. We are unable to obtain detailed information regarding energy disposal for the HO_2 + NO_2 pathway in these experiments. However, it is clear from monitoring total visible fluorescence over the 420−650 nm range, that a substantial amount of the NO_2 fragments is generated in electronic excited states. That these excited NO_2 fragments are indeed being formed from the double-resonance photodissociation of PNA is confirmed by recording an action spectrum that monitors the total visible fluorescence as a function of λ_1 with λ_2 held fixed at 390 nm. Figure 3c shows an action spectrum obtained by this method. The signal-to-noise ratio in this spectra is considerably better than that obtained by monitoring OH fragments in a single quantum state. In fact taking into account the photomultiplier response, filter transmissions, and relative fluorescence signals from NO_2 versus OH, we estimate that the HO_2 + NO_2 channel is at least ~10 times more favored over the OH + NO_3 channel at these excitation energies. This is to be compared with the results at 248 nm, where the yield of the HO_2 + NO_2 channel is ~2 times that of the OH + NO_3 channel.[10] The improved signal to noise associated with monitoring the NO_2 fluorescence in these double-resonance experiments permits us to detect even relatively weak vibrational bands such as the $\nu_1 + 2\nu_3$ combination band (involving O−H stretch and OOH bend) located at 6250 cm^{-1}. One immediate benefit of being able to detect this lower energy combination band is that by comparing the integrated intensities of the $\nu_1 + 2\nu_3$ and $2\nu_1$ bands appearing in the vibrational action spectra with their known integrated infrared absorption cross sections, we can estimate the quantum yield for unimolecular dissociation associated with the $2\nu_1$ state. As noted above, Roehl et al.[6] determined the quantum yield for unimolecular dissociation of several near threshold vibrational levels of PNA as a function of temperature and pressure by comparing the relative yield of HO_2 fragments from these levels with those from the much higher energy $3\nu_1$ band, whose dissociation quantum yield they assumed to be unity. Their experiments relied on using the HO_2 + NO titration reaction to convert HO_2 photofragments to OH for the purposes of monitoring HO_2 fragment yields and, thus, were conducted under conditions of high pressure (>2 Torr). The present experiments provide a complementary method for estimating the unimolecular dissociation quantum yields at low pressure (~70−80 mTorr) in the absence of collisions and without requiring nitric oxide. This is accomplished by noting that the integrated signal intensity, S^i, for the ith vibrational band appearing in the double-resonance action spectrum is directly proportional to the product of the following factors:

$$S^i \propto n_0 \sigma^i_{IR} f^i_S \sigma^i_{UV} \sigma^i_{EM} \quad (4)$$

In the above expression n_0 is the number density of PNA molecules in the excitation volume, σ_{IR} is the band's integrated infrared absorption cross section, f_S is the *fraction of vibrationally excited molecules that survive* and do not undergo unimolecular dissociation, σ_{UV} is the cross section for absorption of UV light by these vibrationally excited molecules, and σ_{EM} is their cross section for producing electronically excited NO_2. Since excitation to the first excited singlet electronic state of HO_2NO_2 involves an n → π^* transition that is primarily localized on the NO_2 chromophore,[10] the Franck−Condon factors associated with electronic excitation are likely to be most sensitive to initial vibrational motion in the parent molecule involving the NO_2 moiety. Since the $2\nu_1$ and $\nu_1 + 2\nu_3$ vibrations involve primarily motion on the OH/HOO portion of PNA, these states are likely to have comparable Franck−Condon factors. In addition, as the OH stretching state is the "bright" state in overtone spectroscopy, it is likely that the intensity of the $\nu_1 + 2\nu_3$ combination band arises from mixing of this state with the "bright" $2\nu_1$ state.[23] This is also consistent with the fact that stretch−bend coupling is very common in many other molecules.[24] Thus assuming that state mixing is strong in vibrationally excited PNA, excitation of these vibrational spectral features having comparable energies is expected, on average, to differ little with regards to either their ability to absorb λ_2 or their propensity for producing excited NO_2 fragments upon double-resonance photodissociation; hence they will have similar values for σ_{UV} and σ_{EM}. Strong state mixing and concomitant statistical behavior also seem reasonable given that the vibrational state density of PNA at energies corresponding to $2\nu_1$ is ~10^3 states/cm^{-1}. Hence, under these conditions taking the ratio of integrated intensities of two spectral features in the action spectra, S^i and S^j, gives:

$$(S^i/S^j) \approx (\sigma^i_{IR}/\sigma^j_{IR})(f^i_S/f^j_S) \quad (5)$$

Thus if the total integrated infrared absorption cross sections are known, then one can determine the unimolecular dissociation quantum yield of one vibrational level relative to another. If in addition one of the vibrational states is nondissociative, so $f^j_S = 1.0$, then the quantum yield for the dissociative state f^i_S, is obtained directly. In PNA the $\nu_1 + 2\nu_3$ band is lower in energy compared to the $2\nu_1$ band by about 650 cm^{-1}, and its

unimolecular dissociation quantum yield is observed to be negligible due to energy constraints. In fact the data of Roehl et al.[6] show that the unimolecular dissociation quantum yield for the $\nu_1 + 2\nu_3$ band is ~6% at room temperature (implying that $f^j_S = 0.94$). Consequently we use the $\nu_1 + 2\nu_3$ band as our reference state and take $f^j_S \approx 1$ for this combination band. Using the experimentally determined integrated intensity ratio for the $\nu_1 + 2\nu_3$ and $2\nu_1$ bands (found to be 0.041 from the action spectra), and their corresponding integrated infrared absorption cross-sections ($2\nu_1$: 9.5×10^{-19} and $\nu_1 + 2\nu_3$: 2.7×10^{-20} cm^2 molecule cm^{-1}),[6] we estimate f^j_S for the $2\nu_1$ band to be ~70%; hence at room temperature its dissociation quantum yield is ~30%. We have examined the extent to which the relative UV absorption probability of the two vibrational levels change with λ_2 by carrying out separate experiments using $\lambda_2 = 367$ nm. Consistent with our assumption that the two vibrational levels exhibit similar behavior in the second step of the double-resonance excitation, the vibrational band intensity ratio did not change when λ_2 was changed from 390 to 367 nm. In addition we have confirmed, through power dependence studies involving the λ_1 laser, that the vibrational band intensity ratio is not affected by saturation of the infrared transitions of the stronger $2\nu_1$ band. Our finding for the $2\nu_1$ dissociation quantum yield is consistent with the earlier results of Roehl et al.,[6] who report a unimolecular dissociation quantum yield of ~27% at room temperature.

Summary

In summary we have used double-resonance excitation to investigate the photochemistry of HO_2NO_2 free from interference of various impurities that are typically present in PNA samples. The combination of $2\nu_1 + 390$ nm used in these state-selected photodissociation experiments corresponds to an effective single-photon excitation of ~307 nm. These first measurements provide information on the energy disposal for the minor OH + NO_3 channel resulting from electronic photodissociation of PNA. The primary channel, associated with the $NO_2 + HO_2$ pathway, is detected through monitoring NO_2 excited-state fluorescence. The NO_2 fluorescence intensity is sufficiently intense to allow us to record action spectra of both the $2\nu_1$ and $\nu_1 + 2\nu_3$ bands. Comparing integrated intensities of these bands appearing in the state-selected action spectra with their known infrared absorption cross section allows us to determine the quantum yield for unimolecular dissociation for the predissociative $2\nu_1$ level. This parameter is important in accessing the infrared initiated photochemistry of HO_2NO_2 in the atmosphere. The present measurements indicate that the states associated with the $2\nu_1$ level that have sufficient energy to undergo unimolecular dissociate at room temperature do so on a time scale faster than ~7 ns. In addition the quantum yield for unimolecular dissociation of the HO_2NO_2 $2\nu_1$ state is determined to be $30 \pm 5\%$ in the absence of collisions at 298 K. The present results are in good agreement with the earlier results of Roehl et al. obtained at high pressure with the $HO_2 + NO \rightarrow OH + NO_2$ reaction to monitor formation of HO_2 from excitation of HO_2NO_2 in the region of the $2\nu_1$ level.[6] In future experiments we hope to use the double-resonance technique to investigate the dependence of HO_2NO_2 unimolecular dissociation quantum yield on temperature.

Acknowledgment. We thank NSF and the academic senate of UCSD for partial support of this work. We thank Melanie McWilliams for assistance on various aspects of the experiment.

References and Notes

(1) Brasseur, G. P.; Orlando, J. J.; Tyndall, G. S. *Atmospheric Chemistry and Global Change*; Oxford University Press: New York, 1999.
(2) Donaldson, D. J.; Frost, G. J.; Rosenlof, K. H.; Tuck, A. F.; Vaida, V. *Geophys. Res. Lett.* **1997**, *24*, 2651.
(3) Donaldson, D. J.; Tuck, A. F.; Vaida, V. *Phys. Chem. Earth C* **2000**, *25*, 223.
(4) Salawitch, R. J.; et al. *Geophys. Res. Lett.* **1994**, *21*, 2551.
(5) Wennberg, P. O.; et al. *Geophys. Res. Lett.* **1999**, *26*, 1373.
(6) Roehl, C. M.; Nizkorodov, S. A.; Zhang, H. G.; Blake, A.; Wennberg, P. O. *J. Phys. Chem. A* **2002**, *106*, 3766.
(7) Molina, L. T.; Molina, M. J. *J. Photochem.* **1981**, *15*, 97.
(8) Knight, G.; Ravishankara, A. R.; Burkholder, J. B. *Phys. Chem. Chem. Phys.* **2002**, *4*, 1432.
(9) DeMore, W. B.; et al. JPL Publication 94-26, NASA/JPL, Pasadena, CA, 1994.
(10) Roehl, C. M.; Mazely, T. L.; Friedl, R. R.; Li, Y.; Francisco, J. S.; Sander, S. P. *J. Phys. Chem. A* **2001**, *105*, 1592.
(11) Macleod, H.; Smith, G. P.; Golden, D. M. *J. Geophys. Res.* **1988**, *93*, 3813.
(12) Zabel, F. *Z. Phys. Chem.* **1995**, *188*, 119.
(13) Staikova, M.; Donaldson, D. J.; Francisco, J. S. *J. Phys. Chem. A* **2002**, *106*, 3023.
(14) Chen, Z.; Hamilton, T. P. *J. Phys. Chem.* **1996**, *100*, 15731.
(15) Zhang, H.; Roehl, C. M.; Sander, S. P.; Wennberg, P. O. *J. Geophys. Res.* **2000**, *105*, 14593.
(16) Calculated using data from ref 14.
(17) Kenley, R. A.; Trevor, P. L.; Lan, B. Y. *J. Am. Chem. Soc.* **1981**, *103*, 2203.
(18) Dutton, G.; Barnes, R. J.; Sinha, A. *J. Chem. Phys.* **1999**, *111*, 4976.
(19) Li, Y.; Francisco, J. S. *J. Chem. Phys.* **2000**, *113*, 7976.
(20) Dixon, D. A.; Feller, D. C.; Zhan, G.; Francisco, J. S. *J. Phys. Chem. A* **2002** *106*, 3191.
(21) Nizkorodov, S. A.; Wennberg, P. O. *J. Phys. Chem.* **2002**, *106*, 855.
(22) Drouin, B. J.; Fry, J. L.; Miller, C. E. *J. Chem. Phys.* **2004**, *120*, 5505.
(23) Nesbitt, D. J.; Field, R. W. *J. Phys. Chem.* **1996**, *100*, 12735.
(24) Quack, M. *Annu. Rev. Phys. Chem.* **1990**, *41*, 839.